

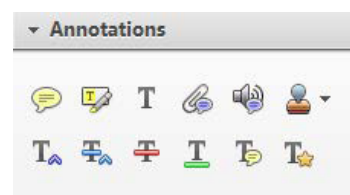
Smart Proof System Instructions

It is recommended that you read all instructions below; even if you are familiar with online review practices.

Using the Smart Proof system, proof reviewers can easily review the PDF proof, annotate corrections, respond to queries directly from the locally saved PDF proof, all of which are automatically submitted directly to **our database** without having to upload the annotated PDF.

- ✓ **Login into Smart Proof** anywhere you are connected to the internet.
- ✓ **Review the proof** on the following pages and mark corrections, changes, and query responses using the **Annotation Tools**.

Note: Editing done by replacing the text on this PDF is not permitted with this application.



- ✓ **Save your proof corrections** by clicking the "Publish Comments" button.
Corrections don't have to be marked in one sitting. You can publish comments and log back in at a later time to add and publish more comments before you click the "Complete Proof Review" button below.
- ✓ **Complete your review** after all corrections have been published to the server by clicking the "Complete Proof Review" button below.

Before completing your review.....

Did you reply to all author queries found in your proof?

Did you click the "Publish Comments" button to save all your corrections?
Any unpublished comments will be lost.

Note: Once you click "Complete Proof Review" you will not be able to add or publish additional corrections.

Bitmap generation from computer-aided design for potential layer-quality evaluation in electron beam additive manufacturing

AQ:au

Hay Wong

School of Engineering, University of Liverpool, Liverpool, UK

Abstract

Purpose – Electron beam additive manufacturing (EBAM) is a popular additive manufacturing (AM) technique used by many industrial sectors. In EBAM process monitoring, data analysis is focused on information extraction directly from the raw data collected in-process, i.e. thermal/optical/electronic images, and the comparison between the collected data and the computed tomography/microscopy images generated after the EBAM process. This paper aims to postulate that a stack of bitmaps could be generated from the computer-aided design (CAD) at a range of Z heights and user-defined region of interest during file preparation of the EBAM process, and serve as a reference image set.

Design/methodology/approach – Comparison between that and the workpiece images collected during the EBAM process could then be used for quality assessment purposes. In spite of the extensive literature on CAD slicing and contour generation for AM process preparation, the method of bitmap generation from the CAD model at different field of views (FOVs) has not been disseminated in detail. This article presents a piece of custom CAD-bitmap generation software and an experiment demonstrating the application of the software alongside an electronic imaging system prototype.

Findings – Results show that the software is capable of generating binary bitmaps with user-defined Z heights, image dimensions and image FOVs from the CAD model; and can generate reference bitmaps to work with workpiece electronic images for potential pixel-to-pixel image comparison.

Originality/value – It is envisaged that this CAD-bitmap image generation ability opens up new opportunities in quality assessment for the in-process monitoring of the EBAM process.

Keywords Prototyping, Quality function deployment, Advanced manufacturing technologies, Layered manufacturing, Image processing, Manufacturing technology

Paper type Research paper



1. Introduction

Electron beam additive manufacturing (EBAM) is a technique which uses an electron beam as a heat source to selectively process metallic powder in a layer-wise fashion. When the electron beam scans across a powder bed in a predefined pattern, melt tracks are formed and cross sections of the desired component are produced. Upon completion of one layer, another layer of powder is deposited onto the processing area, and this building process repeats until the full 3D component is built (Gibson *et al.*, 2010). The EBAM process offers a reduction in thermal residual stress within components (Gong *et al.*, 2014) and a high level of design freedom (Harrysson *et al.*, 2008). This process is popular for manufacturing orthopaedic implants and aerospace components (Baudana *et al.*, 2016). Nevertheless, there are process quality issues, including non-uniform powder layer deposition (Foster *et al.*, 2015), peeled-off metallisation on the processing area (Tor *et al.*, 2014) and component defects (Foster *et al.*, 2015; Tor *et al.*, 2014; Stravroulakis *et al.*, 2016; Sames, 2015). In the

attempt to monitor EBAM process quality, data collection techniques using thermal/optical/electronic in-process imaging have been investigated. Studies were carried out on the Arcam S12 EBM machines by Raplee *et al.* (2017) with a FLIR 7600 mid-wave infrared (IR) camera, and Price *et al.* (2013) with a LumaSense MCS640 near-IR camera. Moreover, Arcam A2 machines were used by Cordero *et al.* (2017) with FLIR SC645 IR cameras, and Scharowsky *et al.* (2012) with a Photron Fastcam SA3 visible light camera. The potential of electronic imaging in EBAM monitoring has also been investigated by both Arnold *et al.* (2018) and Wong *et al.* (2018). Arnold *et al.* (2018) built a backscattered electrons (BSE) imaging system for a modified Arcam S12 EBM machine, whereas Wong *et al.* (2018) developed an electronic imaging system prototype for an Arcam A1 EBM machine.

Regarding data analysis for the evaluation of layer-quality, Raplee *et al.* (2017) evaluated the melting process by analyzing regional slopes in pixel values of the in-process thermal images. The relationship between temperature profile and

The current issue and full text archive of this journal is available on Emerald Insight at: <https://www.emerald.com/insight/1355-2546.htm>



Rapid Prototyping Journal
© Emerald Publishing Limited [ISSN 1355-2546]
[DOI 10.1108/RPJ-05-2019-0146]

The author declares that there is no conflict of interest. This research received no specific grant from any funding agency in the public, commercial, or not-for-profit sectors. The EBAM machine was purchased, in part from a grant received for the EPSRC Centre for Innovative Manufacturing in Additive Manufacturing, EP/I033335/2.

Received 30 May 2019
Revised 11 October 2019
Accepted 16 December 2019

microstructure of components was also investigated. In-process thermal images were compared with post-process electron backscatter diffraction (EBSD) results of the EBAM-manufactured components. Mireles *et al.* (2014, 2015) detected intentional defects using thermal images of an EBAM component via a contour tracing algorithm. These thermal images were also correlated with post-process computed tomography (CT) scan data of the EBAM component to confirm the observation of the thermal imaging system. In other articles, Mireles *et al.* (2014, 2015) detected porosity in EBAM-manufactured components and monitored the EBAM processing area temperature. Comparisons were made between a calculated average pixel intensity (represents an average temperature) from thermal images and the user-pre-defined pixel intensity range (represents the desired temperature range). Rodriguez *et al.* (2012) analyzed the in-process thermal image histograms of the EBAM processing area to identify cold spots. Arnold *et al.* (2018) evaluated the topography and porosity of EBAM-manufactured components. Comparisons were made between in-process electronic images and post-process CT scans and images from an optical microscope. This article postulates an alternative data analysis method – the evaluation of in-process collected data against a set of bitmaps generated from the computer-aided design (CAD) model, which serves as the reference image set.

2. Custom computer-aided design-Bitmap generation software development

3D surface geometries can be represented by triangular tessellation (Milewski, 2017). The American Standard Code for Information Interchange (ASCII) Stereolithography (STL) format, which is used in this study, is one of the tessellation file formats. In this format, each tessellation triangle is described by two pieces of information: the 3 D Cartesian coordinates of the triangle vertices, and the normal unit vector of the triangular plane (pointing outward of the model), as summarised in Table I (Touretzky, 2016).

To prepare for a typical AM process, the STL file of a CAD model first undergoes a slicing operation. The slice depth is set to be equivalent to the AM processing layer thickness, whereas the slice direction is in the AM-build direction. Layers of cross sections of the original 3D design are generated as the output. In a typical AM process, together with the heat source (e.g. laser, electron beam) parameters, the 2D design information is then translated into machine code, the G-code (Kanada, 2016). During manufacturing, this G-code is read by an AM machine, and the AM process is carried out by building the design cross sections with the predefined beam parameters and machine steps, in a layer-by-layer fashion (Franchin *et al.*, 2015).

The purpose of this custom software development is to generate bitmaps from CAD models in the STL format. The

Table I Sample ASCII STL file format (Touretzky, 2016)

Parameter	Value
Triangle facet normal	(n_x, n_y, n_z)
Triangle vertices	$(v_{1x}, v_{1y}, v_{1z}), (v_{2x}, v_{2y}, v_{2z}), (v_{3x}, v_{3y}, v_{3z})$

development is partly built upon an existing Python package called “conformal surfaces” (University of Liverpool, UK) (Robinson, 2014). Part of the “conformal surfaces” source code is used to enable the import of STL files and extraction of the 3D Cartesian coordinates of triangle vertices contained in the STL files. Figure 1 shows the operation on one arbitrary Z plane to give the process flow overview of the CAD-bitmap generation software.

2.1 3D computer-aided design model slicing and 2D contour vector generation

In an STL file, the surface geometry of a design is represented by a set of triangles via meshing. During STL file slicing, the STL segments are analyzed using vector calculus. A set of 2D contours are generated based on a set of Z planes (in typical AM processes, the Z direction is the build direction). Figure 2 and equations 1-4 describe the working principle of the slicing operation carried out by the software.

$$\vec{V}_{SF} = \vec{V}_{OF} - \vec{V}_{OS} \tag{1}$$

$$\vec{V}_{OX} = \vec{V}_{OS} + \vec{V}_{SX} \tag{2}$$

where:

V_{SF} is an arbitrary STL vector segment in a 3D Cartesian space, V_{OS} is the vector connecting the origin and the start point S of V_{SF} , V_{OF} is the vector that connects the origin and the finish point F of V_{SF} , and V_{OX} is the vector connecting the origin and an arbitrary point X in space.

Figure 2 and equations (2) and (3) show that if \vec{V}_{SX} is parallel to \vec{V}_{SF} , then \vec{V}_{SX} can be expressed by $(\vec{V}_{SF})t$, where t is a scale factor.

Figure 1 CAD-bitmap generation overview, for one arbitrary Z plane

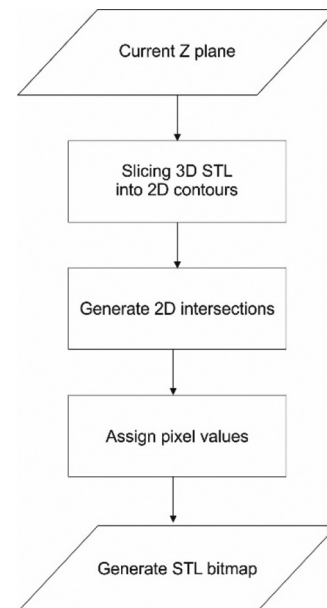


Figure 2 Definition of an STL segment in vector calculus

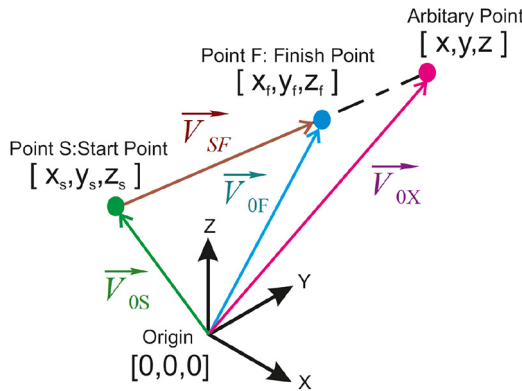
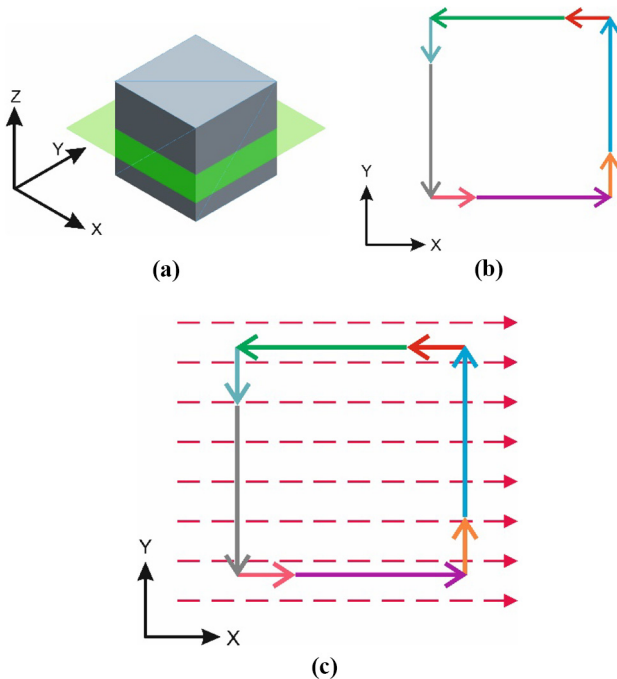


Table II All possible values of "t" during STL slicing

Value of "t"	Implication
$t < 0$	The intersection lies beyond the length of \vec{V}_{SF}
$t = 0$	The intersection is at the start point of \vec{V}_{SF}
$0 < t < 1$	The intersection lies within \vec{V}_{SF}
$t = 1$	The intersection is at the end point of \vec{V}_{SF}
$t > 1$	The intersection lies beyond the length of \vec{V}_{SF}
t cannot be resolved	There is no intersection between the selected Z plane and the arbitrary STL segment \vec{V}_{SF}

Figure 3 2D intersections generation



Notes: (a) STL cube and a selected Z plane; (b) 2D contour vectors; (c) virtual horizontal scan lines, 2D contours and intersections

$$\vec{V}_{0X} = \vec{V}_{0S} + (\vec{V}_{SF})t \quad (3)$$

$$\begin{bmatrix} x \\ y \\ z \end{bmatrix} = \begin{bmatrix} x_S \\ y_S \\ z_S \end{bmatrix} + \begin{bmatrix} x_F - x_S \\ y_F - y_S \\ z_F - z_S \end{bmatrix} t \quad (4)$$

If both the start and finish point of a chosen STL vector segment, \vec{V}_{SF} , are known, it is possible to decide if a selected Z plane intersects with the chosen STL vector segment. With the coordinates of the arbitrary STL segment start and finish points,

Figure 4 Pixel assignment algorithm in detail

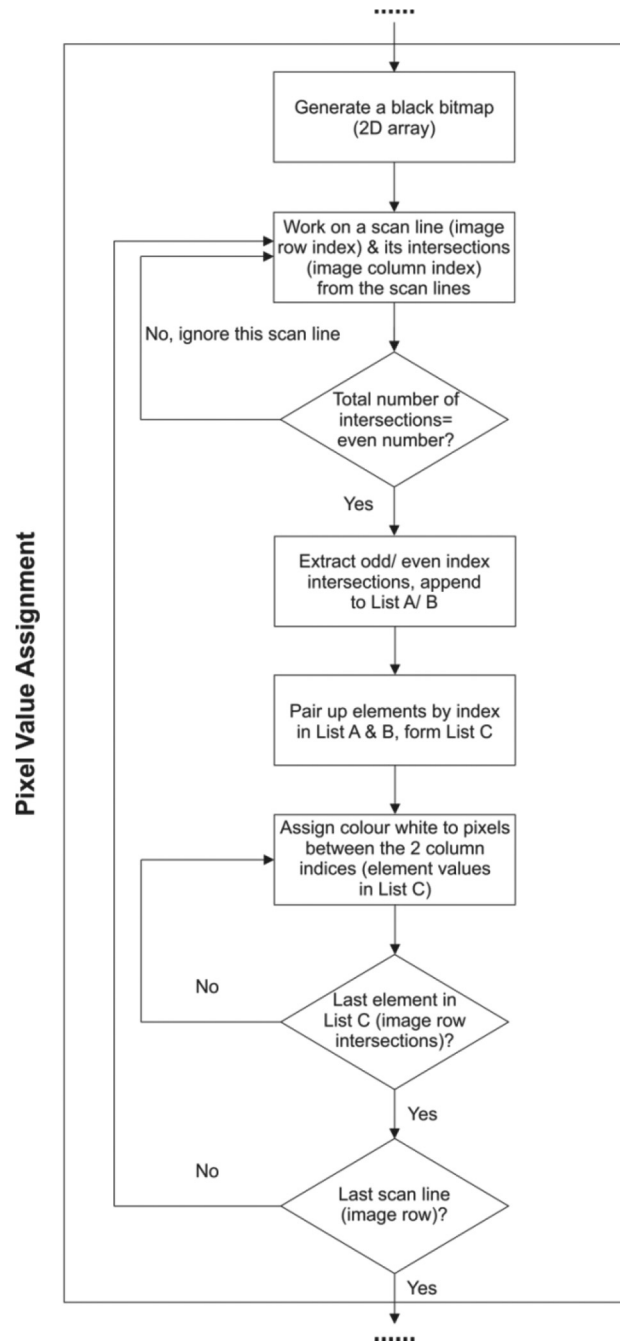
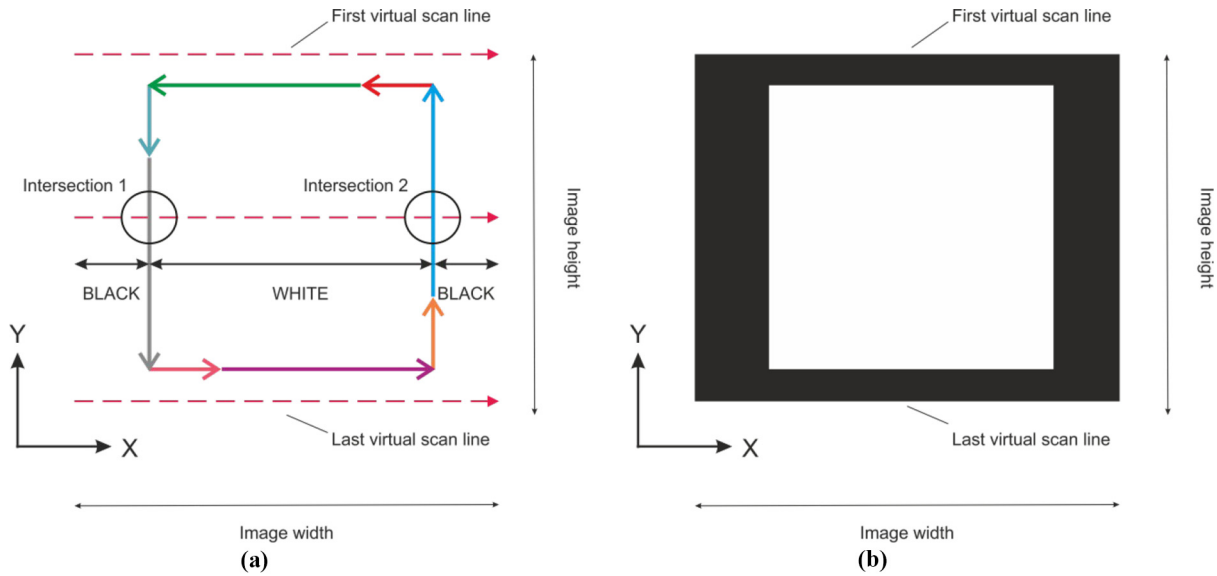


Figure 5 Pixel assignment demonstration



Notes: (a) 2D intersections; (b) resultant binary bitmap

and the Z coordinate of the selected plane known, x_i and y_i of the 3D intersection can be calculated through finding the scale factor “ t .” Table II summarises all possible values for “ t ” and their implications.

2.2 2D intersection generation

Following STL slicing, to generate 2D intersections, virtual scan lines are overlaid on top of the 2D contour vectors (3D intersections from the same STL triangle joint together to form a vector). Figure 3(a) depicts a cube and an arbitrarily selected Z plane. Figure 3(b) illustrates the slicing output: 2D contour vectors which live on the selected Z plane; and Figure 3(c) demonstrates how 2D intersections with virtual horizontal scan lines are defined. The intersections between the 2D contour vectors and the virtual scan lines can be found by applying equation (5), which is a 2D version of equation (4) with a known Y value.

$$\vec{V}_{0X} = \vec{V}_{0S} + (\vec{V}_{SF})t$$

$$\begin{bmatrix} x_n \\ C \end{bmatrix} = \begin{bmatrix} x_S \\ y_S \end{bmatrix} + \begin{bmatrix} x_F - x_S \\ y_F - y_S \end{bmatrix} t \quad (5)$$

where:

C is the known y -coordinate of a scan line, and x_n is the x -coordinate of an intersection between the scan line and a 2D contour vector, which can be found by first resolving for “ t .”

2.3 Pixel value assignment

Following the generation of 2D intersections, to assign pixel values, the 2D intersections on each virtual horizontal scan line are analyzed, as described by process flow chart in Figure 4 (an elaboration of the overview given in Figure 1). The key factor is to only keep the scan lines with an even number of intersections, and discard the rest of the scan lines which only

possesses an odd number of intersections. Figure 5(a) and (b) illustrates this idea with a set of 2D contour vectors of an STL cube. Pixels which lie between the 2D intersections are assigned the colour white, with the rest assigned the colour black. The location, length and number of the virtual scan lines define the output bitmap dimensions (number of image pixel columns and rows). The software allows the user to have full flexibility to define the bitmap dimensions.

2.4 Computer-aided design-Bitmap image generation software verification

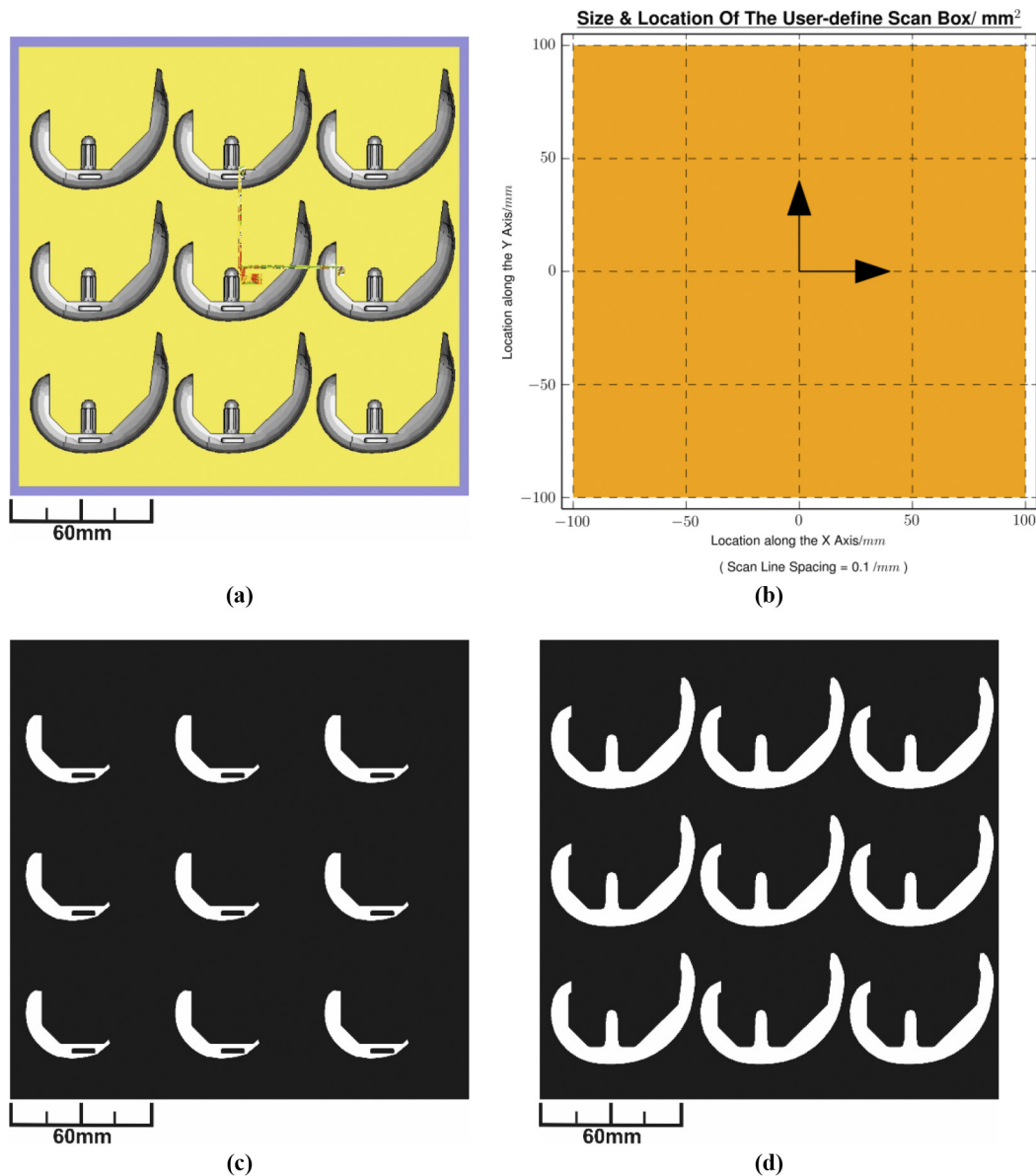
A generic femoral component CAD model (STL format) was obtained from the free online STL database, Thingiverse (www.thingiverse.com). The STL was imported into the Magics software (Materialise NV, Belgium) for re-scaling, populated to fit into a 200 mm \times 200 mm region of interest (ROI), and to align the design frontal plane direction with the origin z -axis in the software. This modified STL was then imported to the image generation software for a software verification trial. Figures 6 and 7 show the resultant bitmaps generated at different:

- user-defined Z heights; and
- field of views (FOVs).

Therefore, the capability of the custom software has been verified.

3. Experimental setup

This section presents the demonstration trial setup. A real-life situation was simulated where the CAD-bitmap generation software was used alongside a digital electronic imaging system prototype for in-process monitoring. The imaging prototype was developed for an Arcam A1 EBAM machine (Arcam AB/GE Additive, USA) (Wong *et al.*, 2018). Figure 8(a) is the schematic of the prototype. The prototype consists of a feedback electron sensor (modified Arcam heat-shield frame and plates), a data

Figure 6 Generic femoral component CAD-bitmap generation (slicing at various Z heights)

Notes: (a) Generic femoral components STL; (b) FOV: 200 mm x 200 mm; (d) 2000 x 2000 pixels, Z = 7 mm; (d) 2000 x 2000 pixels, Z = 17 mm

logger (Arduino DUE microcontroller break-out board), signal amplifier and a piece of electronic image generation software. The prototype was designed to generate digital electronic images from the secondary electrons and backscattered electrons originated from the interactions between the machine's primary electron beam and the processing area. Figure 8(b) shows the imaging target (Wong *et al.*, 2018) used in this experiment. The target was made of Ti-6Al-4V powder, and designed to consist of nine solidified/sintered powder regions.

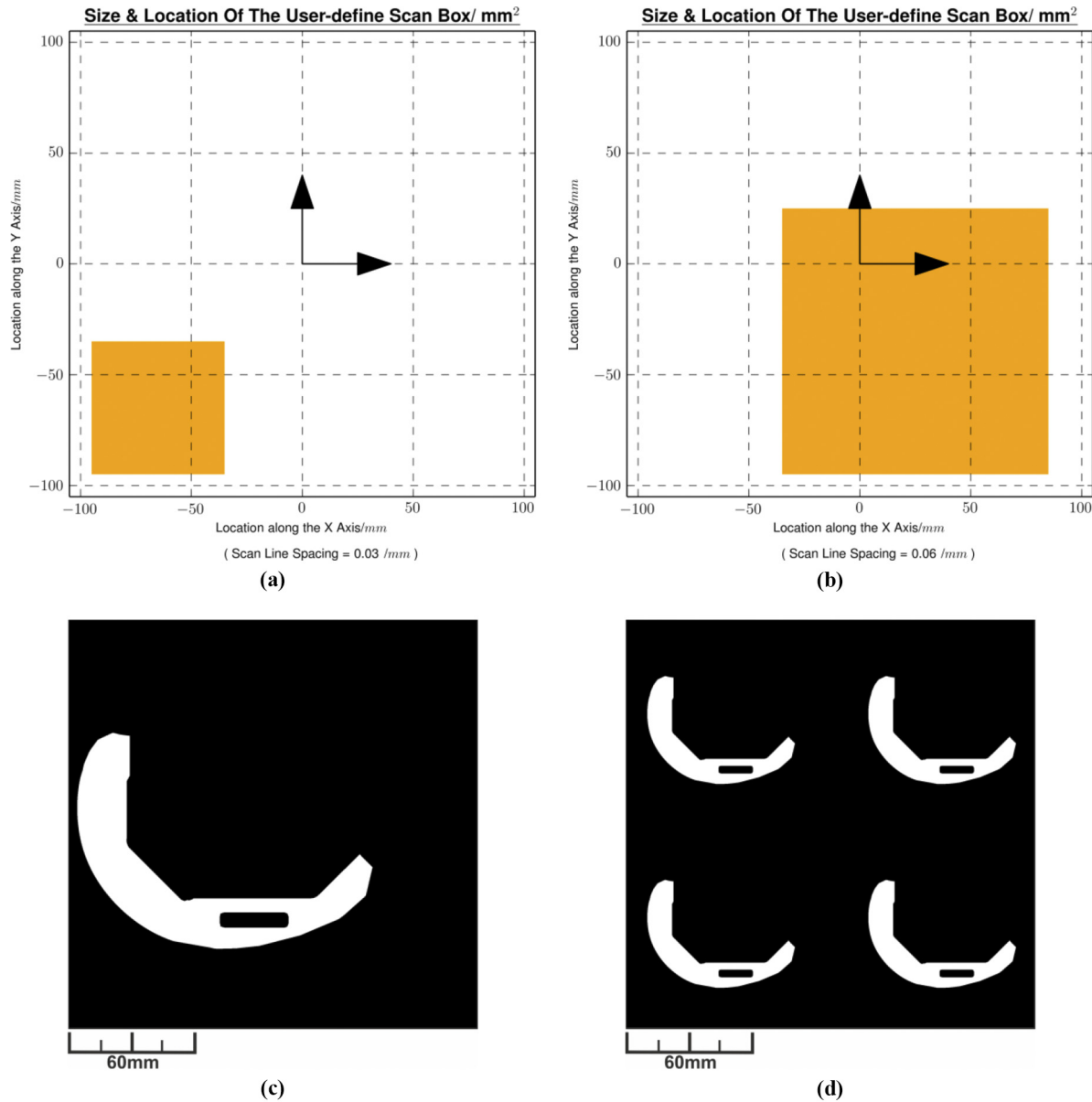
Tables III and IV summarise the experimental configurations and CAD-bitmap generation settings. Tables III and IV show that both the reference image (CAD-bitmap) and the workpiece image (digital electronic image) are set to have the same:

- image dimension; and
- FOV.

This is to allow pixel-to-pixel direct comparison between the reference and workpiece images in data analysis for potential layer-quality evaluation.

In the demonstration, the target was first manufactured by the EBAM machine. Upon completion, the target was taken out of the EBAM machine for excess powder removal in a powder recovery system (Arcam AB/GE Additive, USA). After the removal of excess powder, the imaging target was put back to the EBAM machine processing area. At this point, the CAD-bitmap software generated a reference image according to the settings described in Table IV. After

Figure 7 Generic femoral component at Z = 8 mm (bitmaps from various FOVs)



Notes: (a) FOV: 60 mm x 60 mm; (b) FOV: 120 mm x 120 mm; (c) 2000 x 2000 pixels, lower left; (d) 2000 x 2000 pixels, middle-lower right

that, the imaging prototype carried out electronic imaging according to the configuration set in Table III.

4. Results

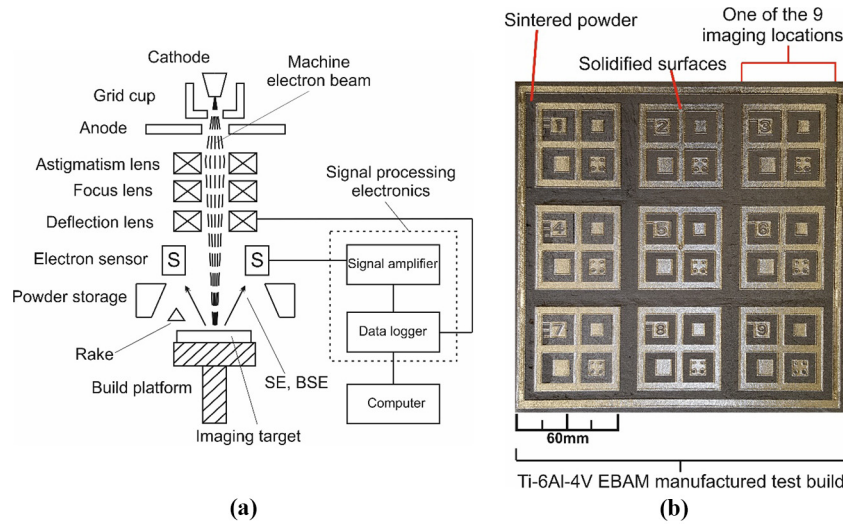
This section presents the results obtained from the demonstration trial. Raw digital electronic workpiece images were generated from location “6” of the imaging target, as illustrated in Figure 9(a) and (c). To generate binary images, image processing was carried out before image thresholding. Noise was removed by applying a median filter, and image contrast was enhanced by carrying out histogram equalisation with the use of the FIJI software (ImageJ, open source).

Equation (6) (Woods and Gonzalez, 2008) and equation (7) (Woods and Gonzalez, 2008) define the median filter and histogram equalisation functions used, respectively. The median filter applied had a user-defined neighbourhood area of a circle with radius of two pixels. The histogram equalisation was carried out with a user-defined saturated pixel value of 0.3 per cent, allowing 0.3 per cent of the total pixels to become saturated.

$$\hat{f}(x,y) = \underset{(s,t) \in S_{xy}}{\text{median}} \{g(s,t)\} \tag{6}$$

where:

F9

Figure 8 Electronic imaging system prototype and the imaging target (Wong et al., 2018)**Notes:** (a) Schematic of the prototype; (b) imaging target**Table III** Arcam A1 EBAM machine and imaging prototype configurations

Parameter	Value
Beam current (mA)	1
Beam scan speed (mm s ⁻¹)	3,960
Chamber pressure (mbar)	2 × 10 ⁻³
Chamber temperature (°C)	30
Image Z height (mm)	14.9
Imaging area (mm ²)	60 × 60 (imaging location "6")
Image size (pixels)	1,800 × 1,800
Image frame time (s)	27.3

Table IV Custom CAD-bitmap generation settings

Parameter	Value
Image Z height (mm)	14.9
Image area (mm ²)	60 × 60 (imaging location "6")
Image size (pixels)	1,800 × 1,800
Image generation time (s)	12.3

$\hat{f}(x,y)$ is the pixel-value of the filtered image at (x,y) , $g(s,t)$ is the pixel-value of the raw image at (s,t) and S_{xy} represents the set of coordinates within a user-defined area of an image.

$$y_k \triangleq \left[\left[(L-1) \sum_{i=0}^k h(i) \right] + 0.5 \right] \quad k = 0, 1, 2, \dots, L-1 \quad (7)$$

where:

L is the bit-depth in an image, k is the pixel-value within the bit-depth, L , $h(i)$ is the normalised histogram which gives the probability of occurrence of pixel-value, L , $\sum h(i)$ is the cumulative probability distribution of the i^{th} normalised histogram, and y_k is an integer, the equalised number of pixel with a pixel-value of k .

Figure 9(d) and (e) shows the processed and binarised electronic images of location "6", respectively. Binary images with the same FOV (location "6") were also generated from the CAD-bitmap generation software, as shown in Figure 9(b) and (f).

5. Discussion

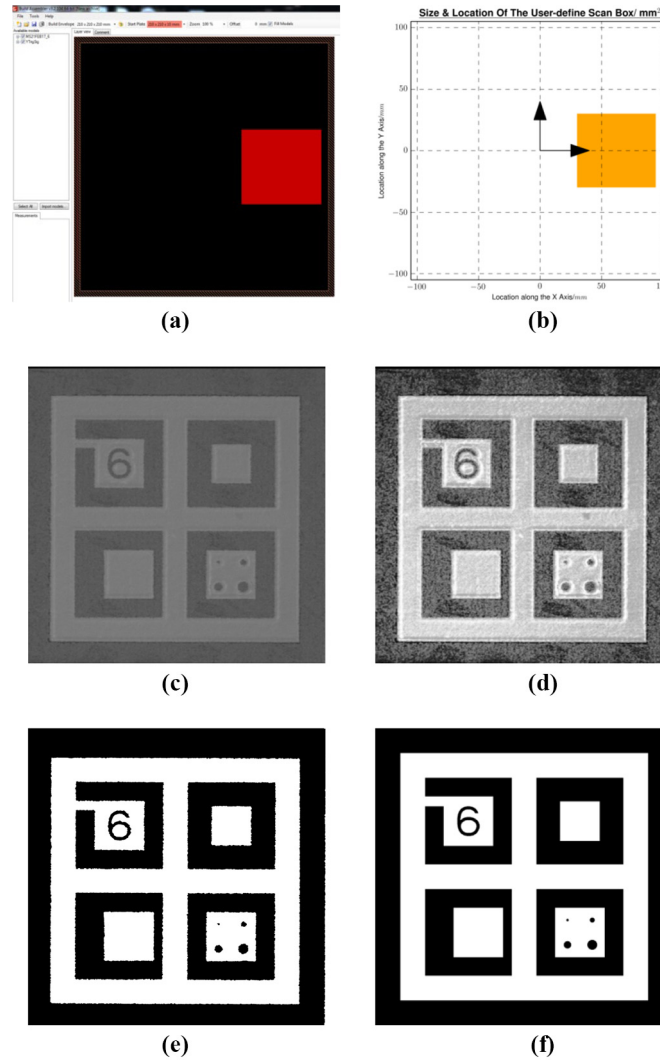
Figure 9(e) and (f) verifies that the CAD-bitmap generation software is capable of generating the same FOV for the bitmap as the electronic image from the imaging prototype. It is thought that these bitmaps, i.e. Figure 9(f), can serve as "reference images", whereas the binarised electronic images, i.e. Figure 9(e) [with the same Z height and FOV as Figure 9(f)], from the prototype serve as "workpiece images." Figure 10 illustrates this concept.

As the reference and workpiece images have the same image dimension and FOV, the pixel-to-pixel image comparison between them is thought to have the potential to reveal typical EBAM process issues, which include, but not limited to, poor powder layer deposition (Foster et al., 2015) and peel-off metallisation fallen onto the processing area (Tor et al., 2014). An "image go/no-go gauge" can be developed based on this pixel-to-pixel comparison. It can then contribute to the decision-making of the acceptance or rejection of a processed EBAM layer. In addition, other metrics could be developed as outlined below:

- a deviation image could be generated for each EBAM layer to reveal the differences in pixel values between a reference and workpiece image when overlaying one on top of the other; and
- a 3D deviation model could be generated from a stack of deviation images generated throughout the EBAM process.

This model could serve as an overall, quantitative feedback to the users on the EBAM-build quality. Although the workpiece electronic image, Figure 9(e), was generated after the EBAM process, this study has showcased the potential for pixel-pixel

Figure 9 Generation of electronic and CAD-bitmap of location "6", after the EBAM process



Notes: (a) Screenshots from the Build Assembler software (Arcam AB)-electronic image FOV; (b) CAD-bitmap FOV; (c) raw electronic image; (d) processed electronic image; (e) binary electronic image; (f) binary CAD-bitmap image

Figure 10 Multi-layer electronic imaging and comparison with CAD-bitmaps (demonstrated with an arbitrary CAD model)

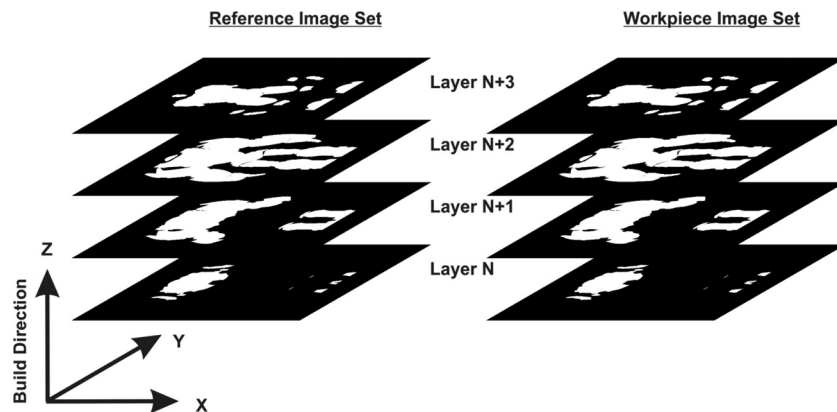


image comparison to be conducted on-the-fly for process monitoring. Live EBAM process monitoring allows machine operators to be notified in the first instance when issues occur. Early discovery of process anomaly saves production cost and time. This is important if the EBAM technique were to gain wider adoption in the manufacturing sector. In spite of the potentials suggested by the experimental results and concepts derived from this study, [Tables III](#) and [IV](#) show that workpiece image frame time is 27.3s whereas the reference image generation time is 12.3s for the current hardware/software setup. Further developments are needed to:

- optimise the CAD model slicing and bitmap generation algorithm to speed up the software; and
- upgrade the data-logging electronics (open-source Arduino microcontroller break-out board) by acquiring an industrial-standard data acquisition system.

6. Conclusions

To contribute to the field of EBAM process monitoring, a method of bitmap generation from CAD models has been presented in this article. The CAD-bitmap software verification results have showcased the ability of the software to generate binary reference images from any user-defined FOVs and Z heights of the processing area. In addition, the demonstration results with the custom electronic imaging prototype have shown the potential of an EBAM layer-quality assessment metric based on pixel-pixel image comparison. There will, however, be challenges ahead to realise this potential. Future studies will need to focus on reducing the reference CAD-bitmap generation time, improving the data-logging speed of the electronic imaging system prototype and fully assess the applicability of this image comparison metric by carrying out in-process data collection under real EBAM building conditions to generate electronic workpiece images on-the-fly. Pixel-pixel comparison between a pair of reference CAD-bitmap and workpiece electronic **image** also needs to be conducted in real time, after the material processing of each EBAM layer, during a real EBAM build.

References

- Arnold, C., Pobel, C., Osmanlic, F. and Körner, C. (2018), "Layerwise monitoring of electron beam melting via backscatter electron detection", *Rapid Prototyping Journal*, Vol. 24 No. 8, pp. 1401-1406, doi: [10.1108/RPJ-02-2018-0034](#).
- Baudana, G., Biamino, S., Ugues, D., Lombardi, M., Fino, P., Pavese, M. and Badini, C. (2016), "Titanium aluminides for aerospace and automotive applications processed by electron beam melting: contribution of politecnico di torino", *Metal Powder Report*, Vol. 71 No. 3, pp. 193-199, doi: [10.1016/j.mprp.2016.02.058](#), ISSN 0026-0657.
- Cordero, P.M., Mireles, J., Ridwan, S. and Wicker, R.B. (2017), "Evaluation of monitoring methods for electron beam melting powder bed fusion additive manufacturing technology", *Progress in Additive Manufacturing*, Vol. 2 Nos 1/2, pp. 1-10, doi: [10.1007/s40964-016-0015-6](#).
- Foster, B.K., Reutzel, E.W., Nassar, A.R., Hall, B.T., Brown, S.W. and Dickman, C.J. (2015), "Optical, layerwise monitoring of powder bed fusion", In *Proceedings of the Solid Freeform Fabrication Symposium*.
- Franchin, G., Kayser, M., Inamura, C., Dave, S., Weaver, J.C., Houk, P., Colombo, P., Yangm, M., Oxman, N., Klein, J. and Stern, M. (2015), "Additive manufacturing of optically transparent glass", *3d Printing and Additive Manufacturing*, Vol. 2, pp. 92-105, doi: [10.1089/3dp.2015.0021](#).
- Gibson, I., Rosen, D.W. and Stucker, B. (2010), *Additive Manufacturing Technologies*, Springer, New York, NY.
- Gong, X., Anderson, T. and Chou, K. (2014), "Review on powder-based electron beam additive manufacturing technology", in *ASME/ISCIE 2012 international symposium on flexible automation*, American Society of Mechanical Engineers Digital Collection, pp. 507-515, doi: [10.1051/mfreview/2014001](#).
- Harrysson, O., Cansizoglu, O., Marcellin-Little, D.J., Cormier, D.R. and West, H.A. (2008), "Direct metal fabrication of titanium implants with tailored materials and mechanical properties using electron beam melting technology", *Materials Science and Engineering: C*, Vol. 28 No. 3, pp. 366-373, doi: [10.1016/j.msec.2007.04.022](#), ISSN 0928-4931.
- Kanada, Y. (2016), "Method for procedural 3D printing using a python library", *Journal of Information Processing*, Vol. 24 No. 6, pp. 908-916, doi: [10.2197/ipsjip.24.908](#).
- Milewski, J.O. (2017), "Additive manufacturing of metals: from fundamental technology to rocket nozzles", *Medical Implants, and Custom Jewelry*, Springer, London, pp. 99-116.
- Mireles, J., Gaytan, S.M., Espalin, D., Wicker, R.B. and Ridwan, S. (2014), "Automatic layerwise acquisition of thermal and geometric data of the electron beam melting process using infrared thermography", in *Proceedings of the Solid Freeform Fabrication Symposium*.
- Mireles, J., Gaytan, S.M., Roberson, D.A., Wicker, R.B. and Terrazas, C. (2015), "Closed-loop automatic feedback control in electron beam melting", *The International Journal of Advanced Manufacturing Technology*, Vol. 78, pp. 1193-1199, doi: [10.1007/s00170-014-6708-4](#).
- Mireles, J., Morton, P., Hinojos, A., Wicker, R.B. and Ridwan, S. (2015), "Analysis and correction of defects within parts fabricated using powder bed fusion technology", *Surface Topography: Metrology and Properties*, Vol. 3, doi: [10.1088/2051-672X/3/3/034002](#).
- Price, S., Lydon, J., Cooper, K. and Chao, K. (2013), "Experimental temperature analysis of Powder-Based electron beam additive manufacturing", *Proceedings from the Solid Freeform Fabrication Symposium*, pp. 162-173.
- Raplee, J., Kirka, M.M., Dinwiddie, R., Okello, A., Dehoff, R. R., Babu, S.S. and Plotkowski, A. (2017), "Thermographic microstructure monitoring in electron beam additive manufacturing", *Scientific Reports*, Vol. 7 No. 1, p. 43554, doi: [10.1038/srep43554](#).
- Robinson, J. (2014), "Optimisation of the selective laser melting process for the production of hybrid orthopaedic devices", PhD thesis, University of Liverpool.
- Rodriguez, E., Espalin, D., Terrazas, C., Muse, D., Henry, C., MacDonald, E., Wicker, R.B. and Medina, F. (2012), "Integration of a thermal imaging feedback control system in electron beam melting", in *Proceedings of the Solid Freeform Fabrication Symposium*.

- Sames, V.W.J. (2015), "Additive manufacturing of inconel 718 using electron beam melting: processing, post-processing, & mechanical properties", PhD thesis, Texas A&M University, Nuclear Engineering.
- Scharowsky, T., Bauereiß, A., Singer, R.F. and Körner, C. (2012), "Observation and numerical simulation of melt Pool dynamic and beam powder interaction during selective electron beam melting", *Proceedings from the Solid Freeform Fabrication Symposium*, Austin, pp. 815-820.
- Stravroulakis, P., Leach, R.K., Clare, A.K., Everton, S.K. and Hirscha, M. (2016), "Review of in-situ process monitoring and in-situ metrology for metal additive manufacturing", *Materials & Design*, Vol. 95, pp. 431-445, doi: [10.1016/j.matdes.2016.01.099](https://doi.org/10.1016/j.matdes.2016.01.099).
- Tor, S.B., Chua, C.K., Tan, X. and Kok, Y. (2014), "Application of electron beam melting (EBM) in additive manufacturing of an impeller", in *Proceeding of the*

- International Conference on Progress in Additive Manufacturing*, doi:[10.3850/978-981-09-0446-3_076](https://doi.org/10.3850/978-981-09-0446-3_076).
- Touretzky, D. (2016), "STL files and slicing software. Teaching materials. 15-294-A4 rapid prototyping technologies spring, computer science carnegie mellon university", available at: www.cs.cmu.edu/afs/cs/academic/class/15294u-s16/
- Wong, H., Neary, D., Shahzad, S., Jones, E., Fox, F. and Sutcliffe, C. (2018), "Pilot investigation of feedback electronic image generation in electron beam melting and its potential for in-process monitoring", *Elsevier Journal of Materials Processing Technology*, doi: [10.1016/j.jmatprotec.2018.10.016](https://doi.org/10.1016/j.jmatprotec.2018.10.016).
- Woods, R.E. and Gonzalez, R.C. (2008), *Digital Image Processing*, Pearson Educaiton, pp. 122-127.

Corresponding author

Hay Wong can be contacted at: hay.wong@liv.ac.uk

For instructions on how to order reprints of this article, please visit our website:

www.emeraldgroupublishing.com/licensing/reprints.htm

Or contact us for further details: permissions@emeraldinsight.com

AUTHOR QUERIES

AUTHOR PLEASE ANSWER ALL QUERIES

AQau— Please confirm the given-names and surnames are identified properly by the colours.

■=Given-Name, ■= Surname

The colours are for proofing purposes only. The colours will not appear online or in print.

